Desalination and Water Treatment
www.deswater.com

doi: 10.5004/dwt.2018.22643

123 (2018) 138–149
August

The role of synthesis method on ZnO nanoparticles: implications for zinc dissolution and arsenite adsorption in water

Mokhtar Ali Amrani[a,*], Asmita S. Gadhaf[b], Nitin K. Labhasetwar[b], Ahmed Sadeq Al-Fatesh[c,*], Sajjad Haider[c,*]

[a]*Faculty of Engineering and Information Technology, Taiz University, 6803 Taiz, Yemen, Tel. +967716186473; email: mokh_ali2007@yahoo.com*
[b]*Energy and Resource Management Division, CSIR-National Environmental Engineering Research Institute (CSIR-NEERI), Nehru Marg, Nagpur 440 020, India*
[c]*Department of Chemical Engineering, College of Engineering, King Saud University, P.O. Box 800, Riyadh 11421, Saudi Arabia, Tel. +966-11-467-6859; Fax: +966-11-467-8770; email: aalfatesh@ksu.edu.sa*

Received 3 October 2017; Accepted 19 June 2018

ABSTRACT

In the recent past, intensive studies have been directed towards the use of zinc oxide nanoparticles (ZnO-NPs) for pollutant uptake and pathogens deactivation from water. However, the chemical behaviour of these suspended colloids in water and their solubility measurements is still not fully understood. Herein, a green synthesis approach was used to fabricate surface-modified ZnO-NPs using *Dracaena cinnabari* (Dragon's blood) extract. A ZnO control sample for comparison was synthesized at similar conditions but without the extract. The obtained powder samples were characterized for structural, morphological and surface properties using various multidisciplinary tools. The environmental stability and adsorption behaviour of surface-modified ZnO-NPs (S1) and pristine ZnO (S2) were studied in aqueous solution at various conditions. S1 sample showed high adsorption capacity for Arsenite (As (III)) and least leaching of Zn ions into water as compared with S2. The results of Zn ions leaching into water (in case of S2) inferred that pristine ZnO sample (S2) was unstable in alkaline and acidic conditions, suggesting its unviability as an adsorbent in most conditions. However, the green synthesis approach for the synthesis of ZnO-NPs has proved a potential step forward towards the safe use of ZnO-NPs for water purification systems.

Keywords: Water purification; Dragon's blood; Dissolution; Green synthesis; Leaching; Adsorption

1. Introduction

Zinc oxide, owing to its unique electronic, optical and surface properties, is one of the most studied metal oxide at nanoscale [1]. It has found widespread applications in environmental, biological and medical fields [1–3]. In the recent past, intensive studies have been directed towards the use of ZnO-NPs for pollutants uptake and pathogens deactivation of water [3–14]. However, the chemical behaviour of ZnO-NPs in water at different conditions is not yet fully explored. Most of the previous studies claimed that high adsorption capacities were attained at strong acidic or alkaline conditions. However, the high solubility of Zn ions and instability of nanocolloids at these conditions were entirely not considered [4–14]. This insufficient research is considered to be the main cause to the growing concerns about the safety use of ZnO-NPs (especially at sizes below 10 nm) to human health and the environment [16]. Some studies, however, proposed that handling some parameters properly would not only make ZnO-NPs stable, less soluble and homogeneously dispersed, but also safer to human health and environment [8,15]. These parameters include size [15–19], shape [19–21], dose [14,22], surface doping with other metals or metal

* Corresponding author.

oxides [22–31] and surface functional groups [7,30–33]. Interestingly, recent studies inferred that microbial biofilm deposition, natural organic matters and ionic strength highly influence the mobility of ZnO-NPs [34–37]. Most of these studies further inferred that the high toxicity of ZnO-NPs is attributed mainly to the high solubility (leaching) of Zn^{2+} ions into the water. Thus, their use as an adsorbent for heavy metals remediation of water could release secondary pollutants (Zn^{2+} ions) into the water system. The Zn leaching into water could be controlled using surface modification with inorganic dopants [13,22–31], and organic functional groups (mostly using surfactants or by applying green synthesis methods) [31–33]. These studies inferred that dopants showed a dramatic decrease in the Zn^{2+} ions leaching into water. Surface coating with various active ligands is a simple method to functionalize metal particles. To this, exploring simple and green methods for the synthesis of uniformly sized and surface-engineered ZnO-NPs (< 10 nm) is still a challenge. Dragon's blood is a unique and rare tree native to Socotra Island, Yemen. Its red resin, extracted from the tree trunk, is known for its medical and antibacterial activity for centuries [38,39]. Structurally, the red resin is rich in several organic antioxidant compounds such as flavonoids, tannins and amino groups. This unique composition enhances the reaction of the electron-rich functionalities (hydroxyls (–OH), carboxyl (C=C), amino ($–NH_2$) groups, etc.) with Zn ions leading to ultrafine and surface-modified ZnO-NPs [38–41].

In our previous study, we have described the use of Dragon's blood extract for the synthesis of surface-engineered Ag/Ag_2O core/shell nanoparticles and their use for As(III) removal [42]. The same synthesis protocol is extended to the preparation of surface-modified ZnO-NPs. The role of synthesis method on ZnO-NPs and their implications for Zn dissolution and Arsenite adsorption in water is also studied. This study clearly inferred that ZnO-NPs synthesized by using Dragon's blood extract (S1) have shown improved As(III) removal and sufficient stable behaviour (least leaching of Zn ions into water) as compared with pristine ZnO particles (S2).

2. Materials and methods

2.1. Materials

Dracaena cinnabari (Dragons' blood) was collected from Socotra Island, Yemen and used as a reducing and stabilizing agent. Zinc chloride ($ZnCl_2$, Sigma Aldrich, India, 98%) and sodium hydroxide (NaOH pellets, Fisher Scientific, India, 98%) were used as a precursor and an alkaline reagent, respectively. Distilled water (Merck Millipore), ethanol and methanol (Alfa Easer, India) were used as solvents. All specified chemicals were of analytical grade and used as received.

2.2. Extract preparation

Dragon's blood extraction methodology was fully described in our previous work [42]. In brief, red resin of the Dragon's blood tree was collected and repeatedly purified with methanol. The purified red resin was collected in a container, dried and stored as a red powder. In the subsequent step, 20 mg of extract powder (red resin) was well-dispersed in 100 mL ethanol for 10 min at room temperature resulting in a red solution.

2.3. Synthesis of ZnO-NPs

In a simple synthesis process, 2.72 g of $ZnCl_2$ was dispersed in 200 mL distilled water and vigorously stirred at room temperature to achieve a homogenous solution. 20 mL of extract solution was added to the previous solution and kept for 1 h until the solution colour was changed to a milky white. During the reaction, the pH of the resultant solution was adjusted at ~9 with the help of NaOH solution. The obtained solution was allowed to precipitate, filtered in a vacuum filtration system, washed several times with water and ethanol and dried at 120°C for 2 h. The ZnO-NPs powder obtained using the extract of the red resin of the Dragon's blood tree was named as S1.

The chelating mechanisms of flavonoids with Zn^{2+} ions have been well-studied in the literature [43–45]. It was argued that flavonoids groups could offer a massive number of nucleation sites for the reduction of Zn^{2+} ions and the formation of ZnO-NPs [46–48]. The reduction process took place mainly via electron donation of the hydroxyl and carboxyl sites [46]. The coordination activity of flavonoids with metal cations is highly enhanced when metals are used in ionic form and in alkaline environments (flavonoids tend to dissolve easily in alkaline water and enhance the antioxidant activity) [47–49]. The same procedure was also adopted for the synthesis of ZnO-NPs using only NaOH (without the use of dragon's blood extract). The $Zn(OH)_2$ precipitates obtained during the reaction were calcinated at 150°C for 2 h to ensure complete dehydration of $Zn(OH)_2$ to ZnO phase. The ZnO-NPs powder obtained by this method was named as S2. After drying (S1) and calcination (S2), both types of the ZnO-NPs powder were well-characterized and stored for further use. The mechanistic pathway of the reaction is shown in the following equations:

$$ZnCl_2 + 2NaOH \rightarrow Zn(OH)_2 + 2NaCl \quad (1)$$

$$Zn(OH)_2 \xrightarrow{Heat} ZnO + H_2O \quad (2)$$

$$Flavonoid - C + Zn(OH)_2 \rightarrow Flavonoid - C + ZnO + H_2O \quad (3)$$

2.4. Solubility/leaching of Zn ion study

The solubility/leaching of Zn^{2+} ions of S1 and S2 samples was studied as a function of contact (10 min–48 h) time, ZnO dose (0.02–1 g L^{-1}) and pH range (3–12). The blank water samples (no ZnO powder added) were used in the experiment. Appropriate amounts of S1 and S2 samples were added to glass flasks. The flasks were tightly closed and exposed to uniform shaking at 150 rpm and 25°C using a shaker (Remi, India). The samples were removed from the shaker at regular time intervals, filtered with 0.22 μm disposable filters, and the concentrations of Zn^{2+} ions in the filtered samples were analysed by inductively coupled plasma mass spectroscopy (ICP-MS, Perkin Elmer, NexIon 300X).

2.5. Effect of pH

To study the effect of surface activity of ZnO adsorbents on the As(III) uptake under varying pH values, experiments were carried at ZnO dose 0.3 g L^{-1}, As(III) concentration 562 μg L^{-1} and contact time 10 min–48 h. S1 and S2 samples (0.3 g L^{-1} of ZnO) were separately added to glass flasks. An appropriate volumes of As(III) concentration 562 μg L^{-1} were also added to glass flasks. The flasks containing suspensions were tightly closed and uniformly shaken at 150 rpm, 25°C and varied pH using an incubator shaker for the required contact time. After shaking the solutions were filtered using 0.22 μm disposable filters. The concentrations of As (III) ions in the filtered samples were then analysed using ICP-MS.

2.6. Zeta potential measurements

Aqueous solutions of ZnO-NPs samples were prepared by the addition of 10 mg L^{-1} of ZnO-NPs to distilled water and then subjected to ultrasonication (*Sonicator, PCi Analytics*) for 30 min. The pH of the stock solution was measured at 6.8 ± 0.1 and monitored by pH meter (OAKION, Eutech Instruments); suspensions were shaken for 30 min to ensure equilibrium. Final pH of the suspensions was measured and point zero charge was determined with Nanosizer SZ-100 (Horiba Scientific, Japan) at 25°C using dynamic light scattering method.

2.7. Effect of adsorption dose and contact time

Adsorbent dose studies were carried out at various adsorbent doses (0.02–1 g L^{-1}), while As(III) concentration was kept unchanged at 527 μg L^{-1} using 250 mL conical flasks. To carry out the batch dose study, 100 mL of each concentration of As(III) solution and a particular adsorbent dose was added into the conical flask. Control solution (without adsorbent) was prepared to determine the initial As(III) concentration (C_o). Kinetics study was conducted at fixed As(III) concentration (~527 μg L^{-1}) and adsorbent dose (0.3 g L^{-1}). The measurements were conducted at different contact times (1 min–48 h). Removal efficiency (R(%)) was calculated according to Eq. (4) and then plotted as a function of time.

$$R(\%) = \frac{(C_o - C_e) \times 100}{C_o} \tag{4}$$

where C_o and C_e are the initial and equilibrium As(III) concentrations in μg L^{-1}, respectively. The amount of As(III) ions adsorbed (Q_e) for S1 and S2 was calculated using Eq. (5).

$$Q_e = \frac{(C_o - C_e)}{W/V} \tag{5}$$

where Q_e is the adsorption capacity measured in mg g^{-1}, while W/V is the adsorbent dose in mg L^{-1}.

3. Characterization studies

Transmission electron microscope (TEM) (Model FEI Technai G^2 S-Twin) operated at an accelerating voltage of 200 kV and field emission electron microscope (FESEM) (Model Hitachi S-570) operating at an accelerating voltage of 5 kV were used to study the morphology of ZnO-NPs samples. The crystallinity and phase structure of the samples were studied using Bruker's X-ray diffractometer (AXS Model D8 Advance System). X-ray diffraction (XRD) patterns were recorded from 20° to 80° using Cu Kα as the X-ray source (λ = 1.54 Å). Fourier-transform infrared (FTIR) spectroscopy (Model: Nicolet 380 of thermo Scientific) was mainly used to identify the surface activity of the particles. UV-vis spectrometer (Jasco-V-670) was used to study the optical response of the samples. Finally, the point zero charge of the ZnO-NPs samples was measured with Nanosizer SZ-100 (Horiba Scientific, Japan) using light scattering method.

4. Results and discussion

4.1. Structure and surface of ZnO-NPs

Fig. 1(a) shows the X-ray diffractograms of ZnO-NPs (S1 and S2 samples). The diffraction patterns show the characteristic peaks at 2θ = 31.68°, 34.29°, 36.16°, 47.39°, 56.50°, 62.74°, 66.30°, 67.89° and 69.07°, which correspond to (100), (002), (101), (102), (110), (103), (200), (112) and (201) planes of ZnO-NPs [50]. All the diffraction peaks are indexed to the hexagonal ZnO (Inorganic Crystal Structure Database code # 75-0576) [50,51]. Since, there appeared no other peaks than the characteristic peak pattern of ZnO; hence, it is believed that ZnO-NPs were in highly pure phase. Furthermore, the broadened peaks verified the ultrafine nature of ZnO-NPs, whereas the high intensity peaks revealed the high crystallinity of ZnO-NPs. The peaks for S1 were broader as compared with S2 sample (Fig. 1(b)), whereas the peaks of S2 were more intense than S1. These results indicated that the crystallites of S1 were finer but less crystalline while that of S2 were larger but highly crystalline. Our argument in favour of the finer size of the S1 particles was complemented by the average crystallite size, which was calculated from the XRD peaks using Scherer equation. The average crystallite sizes calculated by taking the average of the obtained three peaks (as shown in Fig. 1(b)) for S1 and S2 were ~3.81 and ~26.5 nm, respectively.

Fig. 1(c) shows UV-Vis absorption spectroscopic analysis of S1 and S2 samples. The spectra showed single sharp absorption bands at ~361 and ~370 nm corresponding to S1 and S2 samples, respectively. The absorption bands in this range are characteristic of ZnO-NPs [7,52]. The absence of any additional bands in the UV-Vis scan indicates the high purity of ZnO phase [53]. The results also show a small shift of wavelength, which could be attributed mainly to the difference in particle sizes of both ZnO samples [54]. It is fundamentally known that for a specific material, smaller particle sizes show larger band gap [55], which is adequately validated in the present case of ZnO-NPs variable sizes.

Fig. 1(d) depicts the FTIR spectra of S1 and S2 samples in the wavenumber range of 470–4,000 cm^{-1}. The occurrence of a large number of bands for S1 sample implies that these particles are surface-rich with various functional groups of the red resin extract. These functional groups are advantageous since they are plausibly involved in the adsorption of As(III) and in controlling Zn dissolution in water. The stretching bands of ZnO-NPs were observed at 400–900 cm^{-1} range, arising from

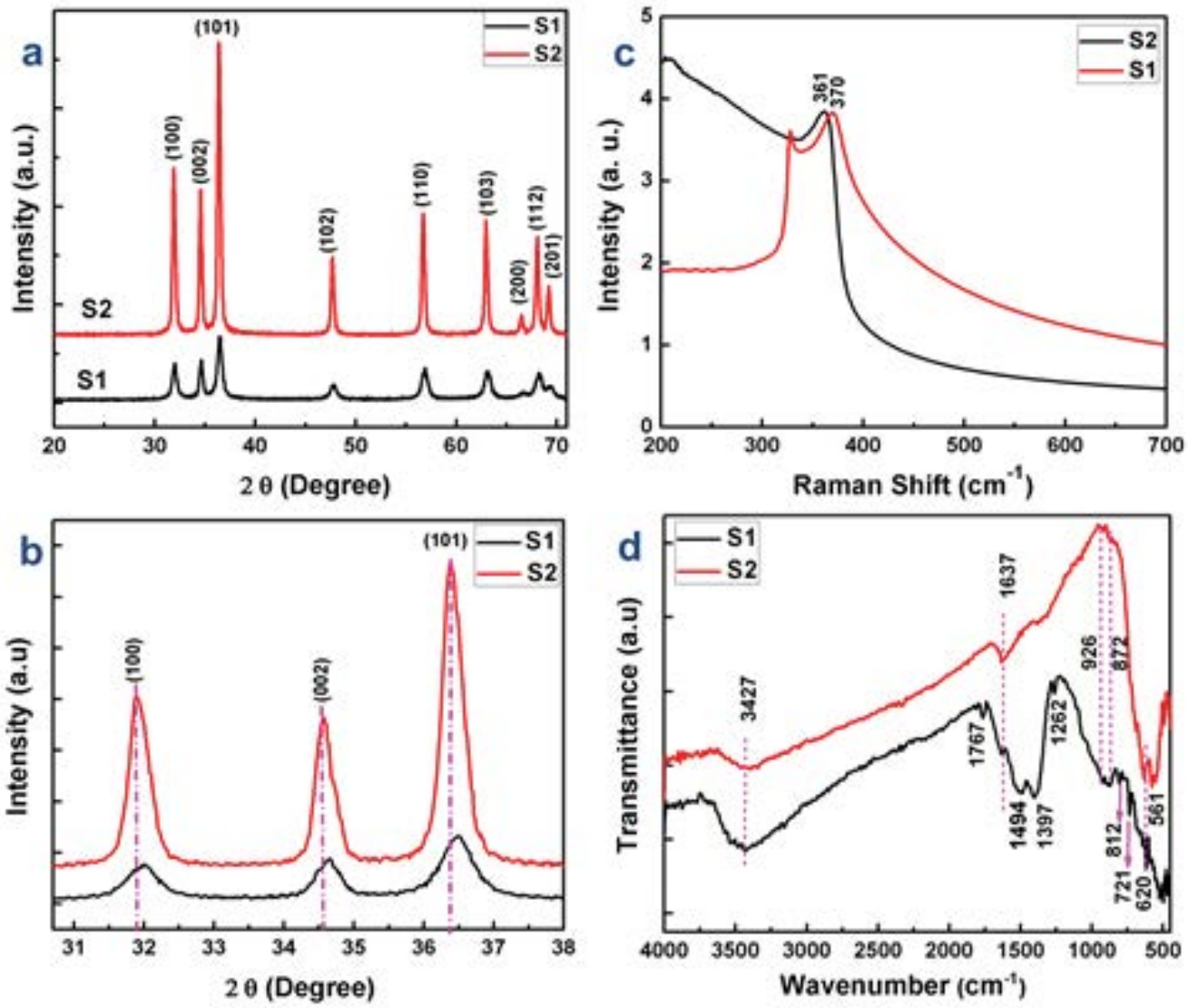

Fig. 1. (a) X-ray diffractograms, (b) high magnification XRD pattern in the 2θ range 31°–38°, (c) UV-vis absorption spectrum and (d) FTIR spectrum of as-synthesized ZnO-NPs using Dragon's blood extract (S1) and ZnO-NPs synthesized using NaOH (S2).

the interatomic vibrations of metal–oxygen bonds [42]. The band at 620 cm^{-1} is attributed to ZnO deformation, which is more intense in the case of S2 sample. The stretching band in the range of 3,400–3,550 cm^{-1} (more intense in the case of S1 sample) is assigned to the hydroxyl group and vapours of water present in the samples [56,57]. The vibrational bands at 1,397, 1,494, 1,637 and 1,767 cm^{-1} are assigned to various symmetric and asymmetric stretching carboxylic groups of different aromatics in the extract [17,56]. In this context, it can be observed that the IR spectra of S1 and S2 samples are not exactly similar. The peaks at 721, 1,262, 1,397, 1,494, 1,767 and 3,515 cm^{-1} are the characteristic bands of S1 sample indicating high contents of antioxidant agents. Instead, FTIR spectrum of S2 sample showed that most of these functional groups are not absorbed to the surface of the particles. The difference in the number of bands and band intensities of S1 and S2 samples concludes that S1 sample contains various surface functional groups.

The estimated surface area values of S1 and S2 samples measured with BET technique were found to be ~23 and ~7 $m^2\ g^{-1}$, respectively. These results indicated that S1 powder has large surface area in comparison with the S2. These findings are compatible with the results of XRD peaks.

4.2. Morphology studies of ZnO-NPs

Fig. 2 shows the morphology and electron diffraction pattern of S1 and S2 samples. TEM images of S1 sample (Figs. 2(a) and (b)) show uniform particles with near spherical shape and narrow size distribution. The average particle size was calculated based on the average of 150 particles to be ~3.29 nm. In contrast, the result obtained from TEM images for S2 sample (Figs. 2(d) and (e)) showed irregular shape particles with a wide size distribution as compared with S1 sample. The large variations of particle shapes and sizes could be attributed mainly to the nature of reducing agent, which

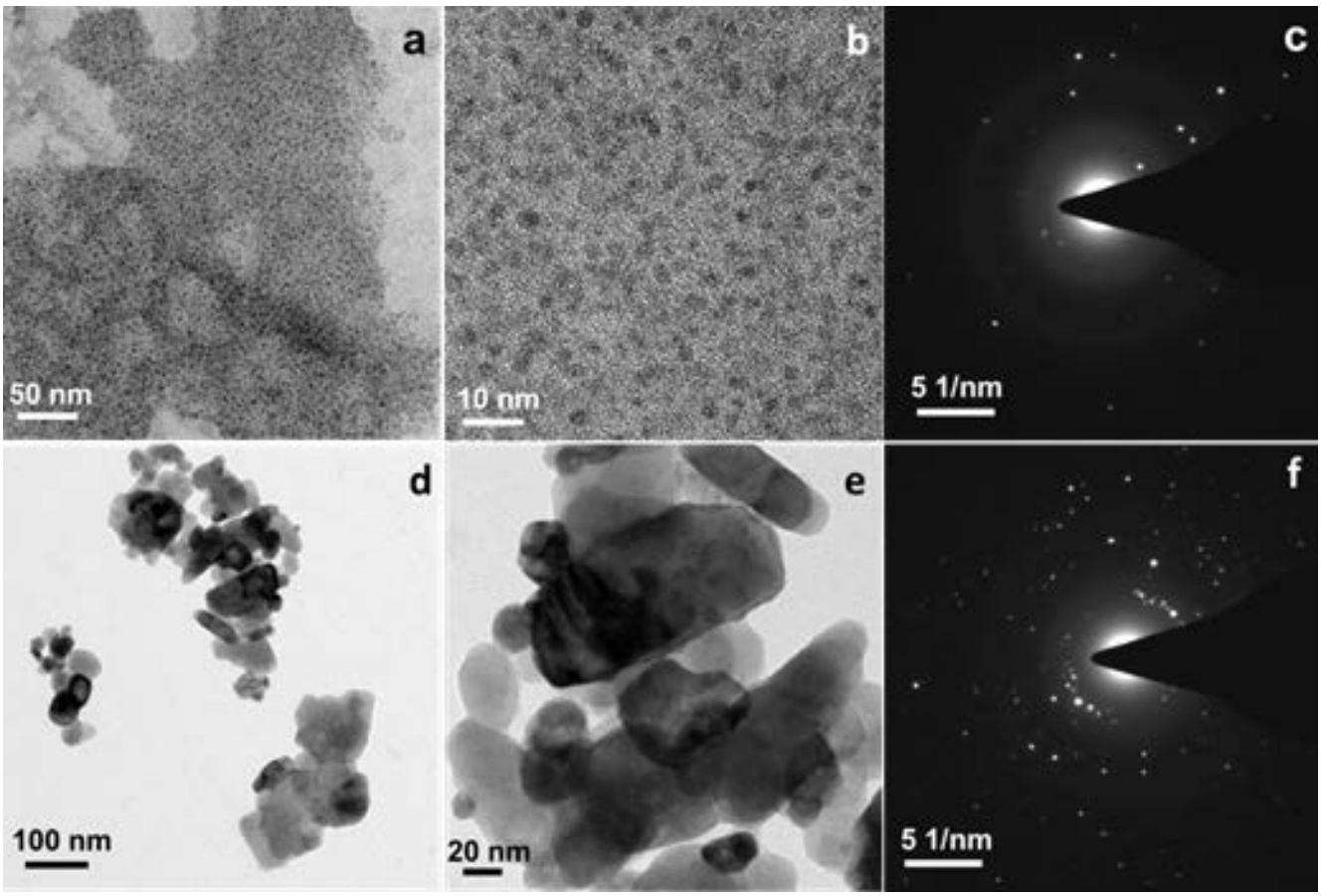

Fig. 2. (a, b) and (d, e) are TEM micrographs showing the geometry of S1 and S2 samples, respectively, (c, f) are SAED patterns of S1 and S2 samples, respectively.

had changed the environment of the nucleation and particle growth. These findings correlate well with the results of XRD patterns of the crystallite size calculated by Scherer equation (Figs. 1(a) and (b)). It is important to know that organic solvent (e.g., ethanol) could enhance the extraction of biologically effective groups by creating a large number of hydroxyl and carboxyl ions, which contribute in numerous secondary reactions leading to the formation of more active functional groups. These groups make chelating sites with Zn ions due to their ability to donate electrons and create complex compounds [58]. Therefore, they nucleate on the surfaces of ZnO-NPs in the early step of the particle growth and hinder the aggregation of the fine particles. The uniform distribution of the ZnO-NPs is attributed to the repulsion forces generated between the particles and phenolic functional groups present in the extract [42,59]. These forces are stronger than the electrostatic attraction forces between adjacent particles themselves. Therefore, uniform and well-dispersed particles were obtained.

Figs. 2(c) and (f) show selected area electron diffraction (SAED) patterns of S1 and S2, respectively. The results confirmed the hexagonal structure of ZnO-NPs and polycrystalline nature of the samples. The results also suggested that the presence of a thin film of functional groups on the surface of ZnO-NPs could alter the crystallinity of particles. Scanning electron micrographs (SEM) of the bulk particles of S1 and S2 samples were shown in Figs. 3(a) and (b), respectively. The features (shapes and size) of the particles were similar to those obtained by TEM micrographs. The particles of S1 sample (Fig. 3(a)) had regular shapes and sizes while the particles of the S2 sample (Fig. 3(b)) had irregular shapes and wide range of particles size distribution. The inset photographs (Fig. 3) are related to S1 and S2 powders. The photographs indicate a slight change of powder colour arising from the red extract, which is plausibly coated on the surface of the particles. These results are in line with the IR results of S1 (Fig. 1(d)).

4.3. Solubility/leaching of Zn into water

Zn is an important trace element in the human body. The daily dietary requirement of Zn is 15–22 mg, ingested mostly throughout the food system [31,60]. The use of ZnO-NPs in the water purification systems attains significance owing to the high acceptable concentration of Zn in drinking water (5 mg L^{-1} based on the World Health Organization (WHO) regulations of drinking water) [60]. More than that, the low cost, bioavailability and easy processing are also advantages for designing real adsorbents based on ZnO-NPs. In contrast, pristine ZnO-NPs are chemically unstable in the water and their transportation rate increases as the particle sizes decreases [15–19]. Hence the use of pristine ZnO-NPs

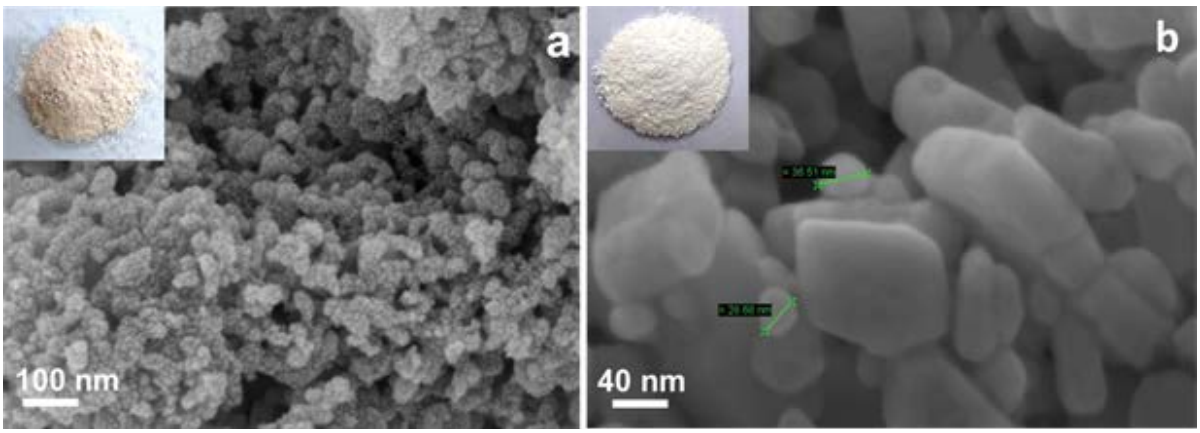

Fig. 3. FESEM micrographs of (a) S1 and (b) S2 samples. Inset figures are photographs of S1 and S2 powders.

as adsorbents for water purification could release secondary pollutants (Zn^{2+}) to the water. Thus, it is imperative to overcome this issue while considering the use of ZnO-NPs as adsorbents in aqueous systems. This section was made exclusively to address the environmental feasibility of ZnO-NPs.

Figs. 4(a)–(d) show the results of solubility/leaching of Zn^{2+} ions from S1 and S2 samples as a function of contact time, ZnO dose and pH altering. The results inferred that the solubility of Zn ions in water is strongly dependent on contact time, pH and ZnO dose. The results also indicated that

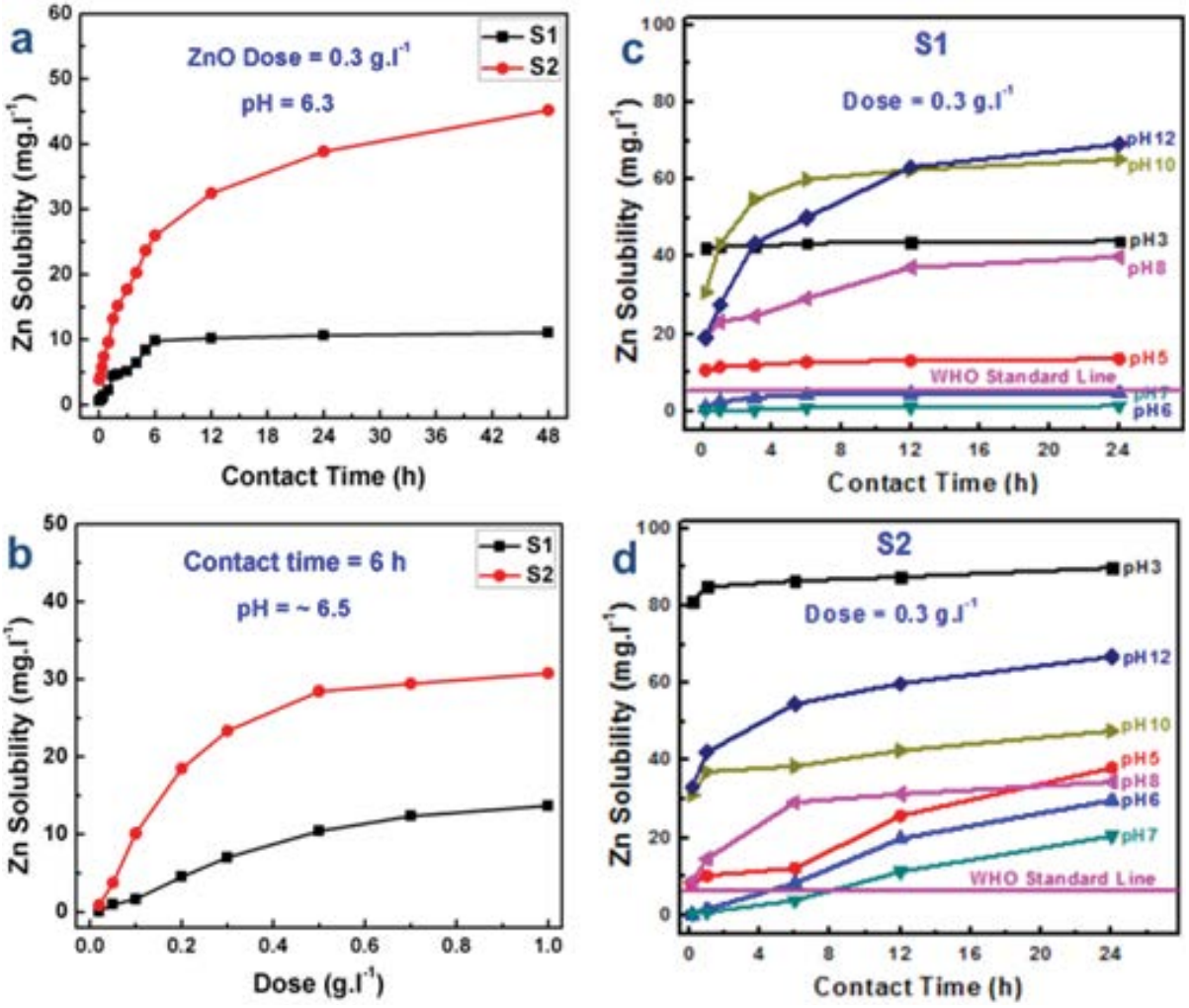

Fig. 4. The effect of (a) contact time, (b) ZnO dose and (c, d) pH measurements of zinc solubility in water for S1 and S2 samples.

S1 showed the least leaching and high stability in water at all studied conditions. The least leaching rate of the S1 could be attributed to the fact that the surface-modified particles had low surface in contact with water molecules due to the presence of active functional groups, which impeded the release of Zn^{2+} ions in water. In fact, the contribution of long contact time (up to 48 h) showed a considerable Zn^{2+} concentration (> 10 mg L^{-1}) in water samples, which indicates the low chemical stability of S1 and S2 samples [59–62]. The results of pH altering showed that the leaching rate of Zn ions from S1 was far less as compared with the S2, plausibly due to the surface protection offered to Zn atoms by a thin film of functional groups as suggested by FTIR results.

The effect of the particle sizes on the solubility of the Zn^{2+} ions into water was unexpectedly different [63]. At a constant pH, the leaching of Zn^{2+} ions of S1 sample (~3 nm size) was observed to be quite low as compared with that of S2 sample (submicron size). These results deviated from a well-known fact that 'smaller particles show larger solubility as compared with larger particles' [14–19]. This deviation was attributed to the fact that the surface-modified particles had a low surface area in contact with water molecules due to the presence of a thin layer of active functional groups, which inhibit the release of more Zn^{2+} ions into water. Therefore, it can be concluded that the green synthesis of ZnO-NPs using plant extract has the following advantages: (1) the synthesis of regular shaped and surface-modified ZnO-NPs, (2) it manipulates the dissolution of Zn^{2+} ions in water and (3) enhances the catalytic activity of the nanoparticles.

4.4. Adsorption studies

4.4.1. pH adsorption study

Figs. 5(a) and (b) show the effect of pH altering on the adsorption of As(III) onto the surface of S1 and S2 adsorbents. These experiments were performed mainly to label the optimum conditions in which As(III) removal is maximized and to clarify whether these conditions are consistent with those of real ground water or not. As discussed earlier in Zn^{2+} solubility/leaching section, the results showed that pH variation is also a critical parameter for adsorption process. The results indicated maximum removal efficiencies for S1 (98.6%) and S2 (89.9%) adsorbents at pH ~5. However, As(III) removal below 10 μg L^{-1} could be achieved using only S1 adsorbent. The results also indicated high removal efficiencies at pH 6 and 7 for both samples. At strong acidic solutions (pH < 5), the negatively charged As(III) ions interact electrostatically with the positively charged ZnO surfaces (the activity of H^+ ions renders ZnO surface more positively) leading to high removal efficiencies. In contrast, extremely low removal efficiencies were observed at strong basic solutions (pH 8–12) for S1 and S2 adsorbents, which could be attributed to the surface erosion of the adsorbent due to excess of OH groups. The formation of zinc hydroxide molecules is soluble in water and considered the main reason for the leaching of Zn ions into water [17]. These results revealed that the use of pristine ZnO-NPs for As(III) uptake at strong acidic and alkaline conditions is not viable.

The adsorption data were also interpreted for the time effect on all studied pH ranges. The results indicated that the adsorption of As(III) onto ZnO samples increased slowly up to 5 h, and reached to equilibrium at ~6 h. At this point the rate of adsorption became equal to the rate of desorption and hence no further adsorption was observed until 48 h. In other words, more than 95% of As(III) was adsorbed onto S1 adsorbent (in the pH range of 5–7) as compared with the S2, where the removal efficiency was only 80%. From the above results, it could be concluded that the surface-modified ZnO-NPs (S1 sample) had high As(III) removal and less leaching of Zn^{2+} ions at circumneutral pH range 5–8 as compared with pristine ZnO-NPs (S2 sample). With recognized enhancements for S1sample, it can be said that both adsorbents were unstable in strong alkaline (pH > 9) and strong acidic (pH < 5) solutions. In fact, intensive studies on the surface modification of ZnO-NPs are further required to improve the NPs chemistry at such conditions.

Fig. 5(c) shows the values of zeta potential (surface charge) as a function of pH. The point of zero charge (PZC) of both samples at different pH was measured by their zeta potential in solution to study their effect on surface charges of ZnO-NPs. The PZC values for surface-coated ZnO-NPs (S1) and pristine ZnO-NPs (S2) were observed at pH 8.3 and 8.0, respectively. This evident difference in PZC values could be assigned to the presence of various functional groups of the extract as suggested by FTIR spectrum for S1 sample (Fig. 1(d)). The plot indicates positive charge of material in an acidic medium and negative charge in an alkaline medium. Furthermore, the results showed that zeta potential (mV) decreases as the pH of the solution is increased. The decrease rate of zeta potential with pH is sharper in the case of S1 than S2. The PZC results obtained for ZnO-NPs in the present study are in close agreement with the literature values 8.0 ± 0.2 [16,64]. However, it was reported that zeta potential parameter for ZnO nanostructures varied over a range of 7–9.5 [16]. This high PZC phenomenon could be ascribed to the surface functional groups from the extract.

4.4.2. Adsorption dose study

Fig. 6(a) depicts the results of adsorption batch study with variable adsorbents (S1 and S2) doses. The experiments aimed to identify the optimum adsorbent dose that is sufficient to effectively decrease As(III) ions in the water below the WHO standards (< 10 μg L^{-1}). The selected range of As(III) concentrations in the present study is consistent with many ground water contaminated sites worldwide [65]. It could be observed from the graph (Fig. 6(a)) that for a water system contaminated with ~500 μg L^{-1} of As(III) ions, the essential S1 and S2 adsorbent doses to attain an equilibrium state (Removal (%) > 96%) were 0.25 and 0.6 g L^{-1}, respectively. These results imply that high removal efficiencies depend not only on the adsorbent dose, but also on the surface properties of the adsorbent particles. The active groups on the surface of ZnO-NPs are advantageous for enhancing the adsorption capacity of the adsorbent, since the surface groups create additional adsorption sites [42]. The results generally inferred that adsorbents based on ZnO-NPs are generally good adsorbents for As(III) uptake, but care must be paid to control the Zn^{2+} leaching to the water system.

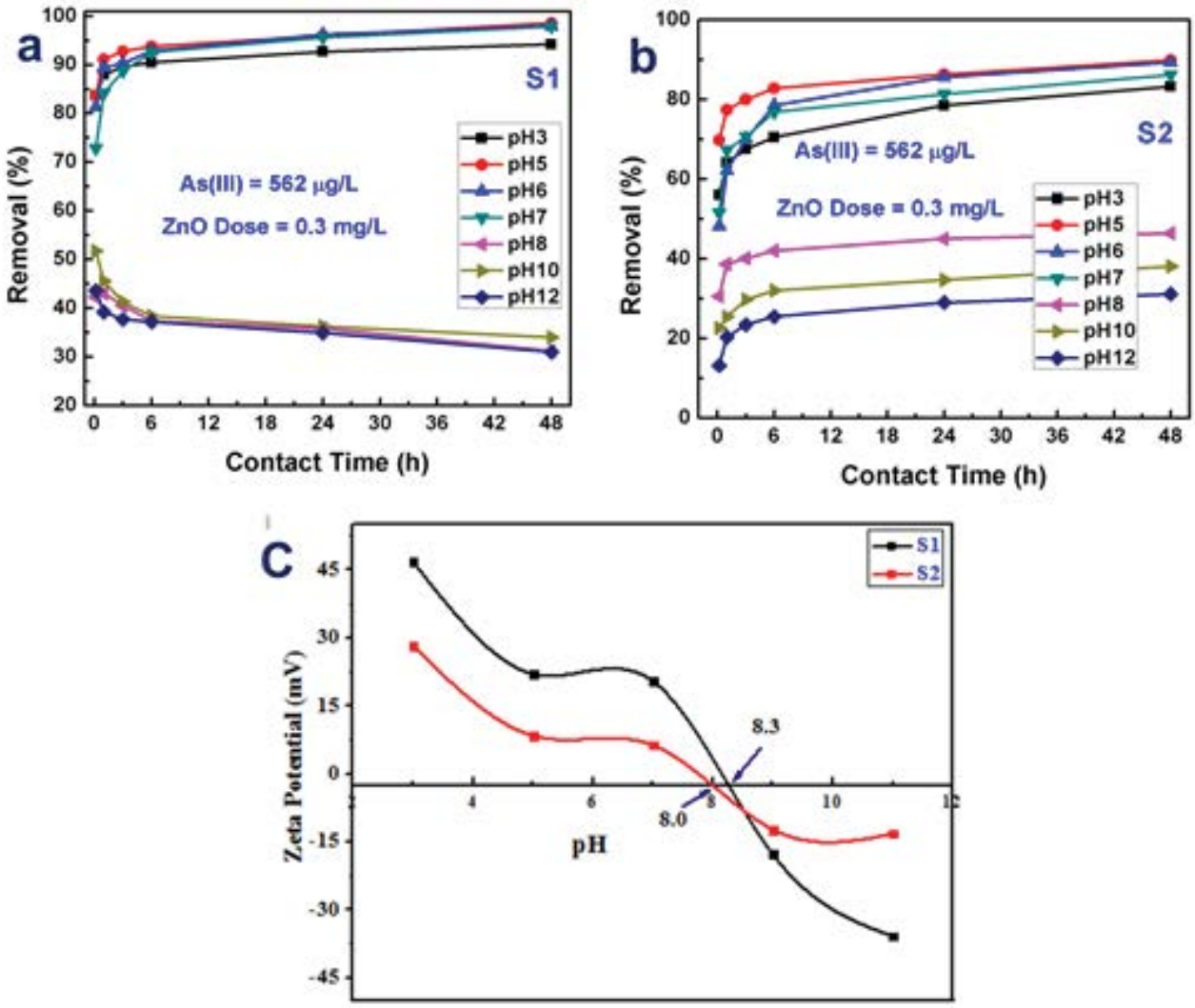

Fig. 5. As(III) removal efficiencies versus contact time at varying pH values using (a) S1 and (b) S2 adsorbents. As(III) concentration and adsorbent dose were kept unchanged during these experiments. (c) Zeta potential of ZnO-NPs suspensions (S1 and S2) at different pH.

4.4.3. Adsorption kinetics

Fig. 6(b) shows the adsorption of As(III) by S1 and S2 adsorbents as a function of contact time. The experiments were conducted using fixed adsorbent doses (0.3 g L^{-1}) and As(III) concentrations (~527 µg L^{-1}). As discussed in the pH effect study, the adsorption of As(III) ions increased slowly until 5 h and reached to equilibrium after 6 h. At this point the rate of adsorption became equal to the rate of desorption and hence plateau was reached, indicating that no further adsorption was observed until 48 h. Unlike S2 adsorbent, which exhibits slow removal (48% in 1 h); S1 adsorbent showed a rapid uptake and more than 90% of As(III) ions were removed in the same period. It is therefore concluded that initially the As(III) ions diffused rapidly into the low energy adsorption sites followed by slow diffusion of As(III) ions at high energy sites [42]. These experiments mutually confirmed the rapid and efficient removal of As(III) onto the surface-modified ZnO-NPs.

4.4.4. Adsorption kinetics models

Adsorption kinetics models are fundamental isotherms to understand the mechanism of the As(III) ions adsorbed onto S1 and S2. The contact time data were analysed by pseudo-first-order (Eq. 6) and pseudo-second-order (Eq. 7) kinetic models. Pseudo-first-order kinetic model is based on physical mass transfer of As(III) ions in which the adsorption rate relates to the unoccupied adsorptive sites. Whereas pseudo-second-order kinetic model describes surface adsorption in terms of chemical interactions between the adsorption sites on the adsorbent surfaces and adsorbate ions [66–69].

$$\log\left(Q_e - Q_t\right) = \log\left(Q_e\right) - K_1 \cdot t \tag{6}$$

$$\frac{t}{Q} = \frac{1}{K_2 \cdot Q_e^2} + \frac{1}{Q_e} t \tag{7}$$

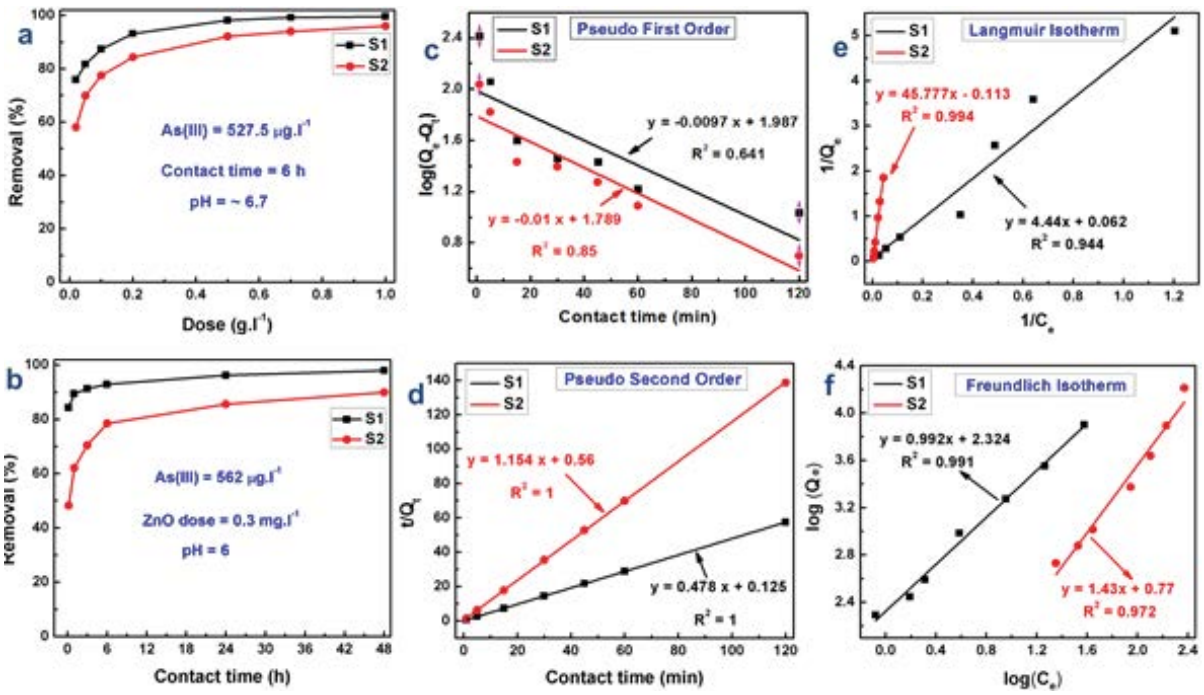

Fig. 6. (a) Adsorption dose study, (b) adsorption time study, (c) pseudo-first-order model, (d) pseudo-second-order model, (e) Langmuir adsorption isotherm and (f) Freundlich adsorption isotherm of ZnO adsorbents (S1 and S2) and As(III) adsorbate.

where Q_t is the amount of As(III) adsorbed at time t (mg g^{-1}), K_1 is the equilibrium rate constant of pseudo-first-order adsorption, K_2 is a pseudo-second-order sorption rate constant (g mg^{-1} min^{-1}) and Q_e is the amount of As(III) adsorbed at equilibrium (mg g^{-1}). K (K_2 and K_1) and Q_e could be calculated from the intercept and slope of the plots of $\log(Q_e–Q_t)$ versus t and t/Q versus t, respectively.

Figs. 6(c) and (d) and Table 1 show that the contact time data did not fit to pseudo-first order. The high linear regression coefficient values (R^2 = 1) recommend that these data followed pseudo-second-order kinetic model, which suggests a chemisorption process where adsorption depends on the number of adsorption sites on ZnO-NPs surfaces [67–69]. In this context, the adsorption can be explained in terms of attractive forces between surface functional groups (hydroxyl, carboxyl and amino groups) and arsenic species.

4.4.5. Langmuir and Freundlich adsorption isotherms

Langmuir adsorption isotherm is a typical method used commonly to estimate the adsorption capacities (Q_{max}) in an adsorbent and to quantify the adsorption mechanism. The linear equation representing Langmuir adsorption is given in Eq. (8) [70].

$$\frac{1}{Q_e}=\left(\frac{1}{Q_{\max}\cdot K_L}\right)\frac{1}{C_e}+\frac{1}{Q_{\max}} \tag{8}$$

where Q_e and Q_{max} (mg g^{-1}) are the equilibrium and maximum adsorption capacities, respectively. K_L (L µg^{-1}) is Langmuir constant. Values of Q_{max} and K_L are calculated from the intercept and slope of the linear plot of $1/C_e$ versus $1/Q_e$ as shown in Fig. 6(e).

The results obtained from the Langmuir plot are represented in Fig. 6(e) and Table 2. Q_{max} values of S1 and S2 adsorbents were calculated to be 16.13 and 8.85 mg g^{-1}, respectively, while K_L values were 0.014 and 0.0025 L µg^{-1}, respectively. Adsorption behaviour can also be expressed using a dimensionless parameter called equilibrium parameter (R_L). The value of R_L relies on the Langmuir constant (K_L)

Table 1
Characteristic kinetics of pseudo-first-order and pseudo-second-order models of ZnO NPs adsorbents and As(III) adsorbate

Pseudo-first-order isotherm			Pseudo-second-order isotherm		
Parameter	S1	S2	Parameter	S1	S2
R^2	0.641	0.85	R^2	1	1
Q_e	7.3	6	Q_e	2.09	0.867
K_1	–0.009	–0.01	K_2	2.38	1.83

Table 2
Langmuir and Freundlich adsorption parameters of ZnO adsorbents (S1 and S2) and As(III) adsorbate

Langmuir adsorption isotherm			Freundlich adsorption isotherm		
Parameter	S1	S2	Parameter	S1	S2
R^2	0.944	0.994	R^2	0.992	0.972
Q_{max} (mg g^{-1})	16.13	8.85	K_f	10.23	2.17
R_L	0.12	0.42	N	0.991	1.43

and initial As(III) concentration (C_o) and can be calculated based on Eq. (9) [71].

$$R_L = \frac{1}{1 + K_L C_o} \tag{9}$$

If value of R_L is between 0 and 1, the adsorption is considered favourable. Since the values of R_L in the present analysis were 0.12 for S1 and 0.42 for S2 adsorbents, hence it is an indication to favourable adsorption.

Freundlich isotherm is also widely used model to explain the way of adsorbate diffusion into adsorbent surfaces. Linear equation representing Freundlich isotherm is given in Eq. (10) [72].

$$\log\left(Q_e\right) = \log\left(K_f\right) + \frac{1}{n}\log\left(C_e\right) \tag{10}$$

where K_f is the specific adsorption capacity in mg g^{-1}, while $1/n$ is the adsorption intensity. The values of K_f and $1/n$ can be obtained from the intercept and slope of the plot log (Q_e) versus log(C_e), respectively. Fig. 6(f) shows the linear regression coefficients of Freundlich isotherm plots (R^2 = 0.995 and 0.972) of adsorbents S1 and S2, respectively. The specific adsorption capacities (K_f) calculated using Freundlich isotherm (Table 2) were found to be 10.23 and 2.17 mg g^{-1} for S1 and S2, respectively. Whereas the values of $1/n$ were calculated to be 0.995 for S1 and 1.43 for S2. In general, $1/n$ values from 0 to 1 give a measure of the degree of heterogeneity of adsorption surface. The closer the value of $1/n$ to 0, the more heterogeneous is the surface and vice versa. Based on the high value of $1/n$ for S1 (0.995) and out of range for S2 (1.43), it can be inferred that S1and S2 adsorption data could be fitted to Langmuir isotherm suggesting monolayer mechanism.

5. Conclusions

A green synthesis approach by using Dragon's blood was conducted to obtain surface-modified ZnO nanostructures with average particle sizes of ~3.5 nm. The results were compared with pristine ZnO particles synthesized at similar conditions but without the extract. XRD results showed pure ZnO phase for both samples. FTIR measurements confirmed the surface ligands of the samples. Electron microscopy confirmed the role of extract molecules on the morphology and crystallinity of particles. The samples were used as adsorbents for the removal of As(III) ions from water and simultaneous measurements of Zn^{2+} ions leaching rate to the water. The results showed that coated ZnO-NPs exhibit high stability in water and strong adsorption affinity as compared with pristine particles at all conditions studied. These improved properties were attributed to the surface functionality of the particles due to the extract effect. Q_{max} of S1 and S2 samples was calculated (based on Langmuir isotherm) at 16.13 and 8.85 mg g^{-1}, respectively. By considering the experimental and isotherm adsorption results, the adsorption of As(III) on to ZnO-NPs suggested a chemical adsorption mechanism (monolayer adsorption). This assumption was also supported by adsorption kinetic results. The results of Zn leaching into water inferred that pristine ZnO adsorbent are unstable in strong alkaline and acidic conditions. This study suggests that for more safety, the use of pristine ZnO-NPs as adsorbents at these conditions is unviable. However, breakthrough impeding of ZnO leaching to water via surface functionalizing suggested safe use of ZnO NPs for water purification systems. More studies in this context are also recommended for minimizing Zn^{2+} ions' leaching and therefore ensuring safe use of ZnO in water interface systems.

Acknowledgements

The authors would like to extend their sincere appreciation to the Deanship of Scientific Research at King Saud University, Riyadh, Saudi Arabia, for its funding for this research group project no. RGP-1435-078. The authors sincerely thank Centre of Nanotechnology, University of Hyderabad, Hyderabad, Telangana, India, for permitting us to use the TEM facility. A part of this work was carried out under the Clean Water project number ESC0306 of CSIR, India and Department of Science & Technology, India under DST-Inspire fellowship.

References

[1] A. Janotti, C.G. Van de Walle, Fundamentals of zinc oxide as a semiconductor, Rep. Prog. Phys., 72 (2009) 126501–126530.
[2] A.K. Radzimska, T. Jesionowski, Zinc oxide – from synthesis to application: a review, Materials, 7 (2014) 2833–2881.
[3] Ing.J. Vymazal, Occurrence and chemistry of zinc in freshwaters – its toxicity and bioaccumulation with respect to algae: a review. Part 1: occurrence and chemistry of zinc in freshwaters, Clean Soil Air Water, 13 (1985) 627–654.
[4] P.Z. Ray, H.J. Shipley, Inorganic nano-adsorbents for the removal of heavy metals and arsenic: a review, RSC Adv., 5 (2015) 29885–29907.
[5] X. Wang, W. Cai, S. Liu, G. Wang, Z. Wu, H. Zhao, ZnO hollow microspheres with exposed porous nanosheets surface: structurally enhanced adsorption towards heavy metal ions, Colloids Surf., A, 422 (2013) 199–205.
[6] S. Srivastava, Y. Srivastav, Removal of arsenic from waste water by using ZnO nano-materials, J. Mater. Sci. Eng. B, 3 (2013) 483–492.
[7] H. Hallaji, A.R. Keshtkar, M.A. Moosavian, A novel electrospun PVA/ZnO nanofiber adsorbent for U(VI), Cu(II) and Ni(II) removal from aqueous solution, J. Taiwan Inst. Chem. Eng., 46 (2015) 109–118.
[8] N. Singh, S.P. Singh, V. Gupta, H.K. Yadav, T. Ahuja, S.S. Tripathy, Rashmi, A process for the selective removal of arsenic from contaminated water using acetate functionalized zinc oxide nanomaterials, Environ. Prog. Sustainable Energy, 32 (2013) 1023–1029.
[9] J. Majeed, J. Ramkumar, S. Chandramouleeswaran, O.D. Jayakumar, A.K. Tyagi, Kinetic modeling: dependence of structural and sorption properties of ZnO-crucial role of synthesis, RSC Adv., 3 (2013) 3365–3373.
[10] X. Wang, W. Cai, Y. Lin, G. Wang, C. Liang, Mass production of micro/nanostructured porous ZnO plates and their strong structurally enhanced and selective adsorption performance for environmental remediation, J. Mater. Chem., 20 (2010) 8582–8590.
[11] S.P. Hernandez, M. Chiappero, N. Russo, D. Fino, A novel ZnO-based adsorbent for biogas purification in H_2 production systems, Chem. Eng. J., 176 (2011) 272–279.
[12] T. Sheela, Y.A. Nayaka, R. Viswanatha, S. Basavanna, T.G. Venkatesha, Kinetics and thermodynamics studies on the adsorption of Zn(II), Cd(II) and Hg(II) from aqueous solution using zinc oxide nanoparticles, Powder Technol., 217 (2012) 163–170.
[13] H. Xu, L. Li, H. Lv, X. Liu, H. Jiang, pH-dependent phosphatization of ZnO nanoparticles and its influence on subsequent lead sorption, Environ. Pollut., 208 (2016) 723–731.

[14] S.B. Khan, M.M. Rahman, H.M. Marwani, A.M. Asiri, K.A. Alamry, An assessment of zinc oxide nanosheets as a selective adsorbent for cadmium, Nanoscale Res. Lett., 8 (2013) 377–384.
[15] M. Ates, J. Daniels, Z. Arslan, I.O. Farah, H.F. Rivera, Comparative evaluation of impact of Zn and ZnO nanoparticles on brine shrimp (*Artemia salina*) larvae: effects of particle size and solubility on toxicity, Environ. Sci. Process. Impacts, 15 (2013) 225–233.
[16] S.W. Bian, I.A. Mudunkotuwa, T. Rupasinghe, V.H. Grassian, Aggregation and dissolution of 4 nm ZnO nanoparticles in aqueous environments: influence of pH, ionic strength, size, and adsorption of humic acid, Langmuir, 27 (2011) 6059–6068.
[17] I.A. Mudunkotuwa, T. Rupasinghe, C.M. Wu, V.H. Grassian, Dissolution of ZnO nanoparticles at circumneutral pH: a study of size effects in the presence and absence of citric acid, Langmuir, 28 (2012) 396–403.
[18] S. Bandyopadhyay, G. Plascencia-Villa, A. Mukherjee, C.M. Rico, M.J. Yacamán, J.R. Peralta-Videa, J.L. Gardea-Torresdey, Comparative phytotoxicity of ZnO NPs, bulk ZnO, and ionic zinc onto the alfalfa plants symbiotically associated with *Sinorhizobium meliloti* in soil, Sci. Total Environ., 515 (2015) 60–69.
[19] D. Xiong, T. Fang, L. Yu, X. Sima, W. Zhu, Effects of nano-scale TiO_2, ZnO and their bulk counterparts on zebrafish: acute toxicity, oxidative stress and oxidative damage, Sci. Total Environ., 409 (2011) 1444–1452.
[20] I.L. Hsiao, Y.J. Huang, Effects of various physicochemical characteristics on the toxicities of ZnO and TiO_2 nanoparticles toward human lung epithelial cells, Sci. Total Environ., 409 (2011) 1219–1228.
[21] R. Bacchetta, B. Maran, M. Marelli, N. Santo, P. Tremolada, Role of soluble zinc in ZnO nanoparticle cytotoxicity in *Daphnia magna*: a morphological approach, Environ. Res., 148 (2016) 376–385.
[22] M. Li, D. Lin, L. Zhu, Effects of water chemistry on the dissolution of ZnO nanoparticles and their toxicity to *Escherichia coli*, Environ. Pollut., 173 (2013) 97–102.
[23] X. Feng, Y. Yan, B. Wan, W. Li, D.P. Jaisi, L. Zheng, J. Zhang, F. Liu, Enhanced dissolution and transformation of ZnO nanoparticles: the role of inositol hexakisphosphate, Environ. Sci. Technol., 50 (2016) 5651–5660.
[24] J. Lv, S. Zhang, L. Luo, W. Han, J. Zhang, K. Yang, P. Christie, Dissolution and microstructural transformation of ZnO nanoparticles under the influence of phosphate, Environ. Sci. Technol., 46 (2012) 7215–7221.
[25] T. Xia, Y. Zhao, T. Sager, S. George, S. Pokhrel, N. Li, D. Schoenfeld, H. Meng, S. Lin, X. Wang, M. Wang, Z. Ji, J.I. Zink, L. Madler, V. Castranova, A.E. Nel, Decreased dissolution of ZnO by iron doping yields nanoparticles with reduced toxicity in the rodent lung and zebrafish embryos, ACS Nano, 5 (2011) 1223–1235.
[26] S. George, S. Pokhrel, T. Xia, B. Gilbert, Z. Ji, M. Schowalter, A. Rosenauer, R. Damoiseaux, K.A. Bradley, L. Madler, A.E. Nel, Use of a rapid cytotoxicity screening approach to engineer a safer zinc oxide nanoparticle through iron doping, ACS Nano, 4 (2010) 15–29.
[27] H. Yin, P.S. Casey, Effects of iron or manganese doping of ZnO nanoparticles on their dissolution, ROS generation and cytotoxicity, RSC Adv., 4 (2014) 26149–26157.
[28] M. Ramasamy, M. Das, S.S. An, D.K. Yi, Role of surface modification in zinc oxide nanoparticles and its toxicity assessment toward human dermal fibroblast cells, Int. J. Nanomed., 9 (2014) 3707–3718.
[29] R. Ma, C. Levard, F.M. Michel, G.E. Brown, Jr., G.V. Lowry, Sulfidation mechanism for zinc oxide nanoparticles and the effect of sulfidation on their solubility, Environ. Sci. Technol., 47 (2013) 2527–2534.
[30] H. Yin, R. Chen, P. Casey, P.C. Ke, T.P. Davis, C. Chen, Reducing the cytotoxicity of ZnO nanoparticles by pre-formed protein corona in supplemented cell culture medium, RSC Adv., 5 (2015) 73963–73973.
[31] J. Zhang, R. Zhang, L.H. Zhao, S.Q. Sun, Synthesis of water-soluble γ-aminopropyl triethoxysilane-capped ZnO:MgO nanocrystals with biocompatibility, CrystEngComm, 14 (2012) 613–619.
[32] M. Luo, C. Shen, B.N. Feltis, L.L. Martin, A.E. Hughes, P.F.A. Wright, T.W. Turney, Reducing ZnO nanoparticle cytotoxicity by surface modification, Nanoscale, 6 (2014) 5791–5798.
[33] V. Merdzan, R.F. Domingos, C.E. Monteiro, M. Hadioui, K.J. Wilkinson, The effects of different coatings on zinc oxide nanoparticles and their influence on dissolution and bioaccumulation by the green alga, *C. reinhardtii*, Sci. Total Environ., 488 (2014) 316–324.
[34] X. Jiang, M. Tong, R. Lu, H. Kim, Transport and deposition of ZnO nanoparticles in saturated porous media, Colloids Surf., A, 401 (2012) 29–37.
[35] R.A. Silva, D. Borja, G. Hwang, G. Hong, V. Gupta, S.A. Bradford, Y. Zhang, H. Kim, Analysis of the effects of natural organic matter in zinc beneficiation, J. Cleaner Prod., 168 (2017) 814–822.
[36] X. Jiang, X. Wang, M. Tong, H. Kim, Initial transport and retention behaviors of ZnO nanoparticles in quartz sand porous media coated with *Escherichia coli* biofilm, Environ. Pollut., 174 (2013) 38–49.
[37] X. Jiang, M. Tong, H. Kim, Influence of natural organic matter on the transport and deposition of zinc oxide nanoparticles in saturated porous media, J. Colloid Interface Sci., 386 (2012) 34–43.
[38] Y.S. Al-Awthan, M. Abu Zarga, S. Abdalla, Flavonoids content of *Dracaena cinnabari* resin and effects of the aqueous extract on isolated smooth muscle preparations, perfused heart, blood pressure and diuresis in the rat, Jordan J. Pharm. Sci., 3 (2010) 8–17.
[39] A. Alwashli, M. Al-Sobarry, Y. Cherrah, K. Alaoui, Anti-inflammatory and analgesic effects of ethanol extract of *Dracaena cinnabari* balf, as endemic plant in Yemen, Int. J. Pharma Bio Sci., 3 (2012) 97–106.
[40] M. Masaoud, H. Ripperger, A. Porzel, G. Adam, Flavonoids of dragon's blood from *Dracaena cinnabari*, Phytocher. Phytochem., 38 (1995) 745–749.
[41] R. Vesela, K. Marek, K. Ubik, K. Lunerova, V. Sklenar, V. Suchy, Dracophane, a metacyclophane derivative from the resin of *Dracaena cinnabari* balf, Phytochemistry, 61 (2002) 967–970.
[42] M.A. Amrani, A. Abu-Taleb, N. Remalli, M. Abdullah, V.V.S.S. Srikanth, N.K. Labhasetwar, Dragon's blood-aided synthesis of Ag/Ag_2O core/shell nanostructures and Ag/Ag_2O decked multi-layered graphene for efficient As(III) uptake from water and antibacterial activity, RSC Adv., 6 (2016) 44145–44153.
[43] Y. Wei, M. Guo, Zinc-binding sites on selected flavonoids, Biol. Trace Elem. Res., 161 (2014) 223–230.
[44] R.F. De Souza, W.F. De Giovani, Synthesis, spectral and electrochemical properties of Al(III) and Zn(II) complexes with flavonoids, Spectrochim. Acta, Part A, 61 (2005) 1985–1990.
[45] C. Lapouge, L. Dangleterre, J.P. Cornard, Spectroscopic and theoretical studies of the Zn(II) chelation with hydroxyflavones, J. Phys. Chem. A, 110 (2006) 12494–12499.
[46] J. Parellada, G. Suárez, M. Guinea, Inhibition of zinc metallopeptidases by flavonoids and related phenolic compounds: structure-activity relationships, J. Enzyme Inhib., 13 (1998) 347–359.
[47] L. Mira, M.T. Fernandez, M. Santos, R. Rocha, M.H. Florencio, K.R. Jennings, Interactions of flavonoids with iron and copper ions: a mechanism for their antioxidant activity, Free Radical Res., 36 (2002) 1199–2208.
[48] Y.S. Tarahovsky, Y.A. Kim, E.A. Yagolnik, E.N. Muzafarov, Flavonoid–membrane interactions: involvement of flavonoid–metal complexes in raft signalling, Biochim. Biophys. Acta, 1838 (2014) 1235–1246.
[49] M.E. Bodini, M.A.D. Valle, R. Tapia, F. Leighton, P. Berrios, Zinc catechin complexes in aprotic medium. Redox chemistry and interaction with superoxide radical anion, Polyhedron, 20 (2001) 1005–1009.
[50] Z. Dai, K. Liu, Y. Tang, X. Yang, J. Bao, J. Shen, A novel tetragonal pyramid-shaped porous ZnO nanostructure and its application in the biosensing of horseradish peroxidase, J. Mater. Chem., 18 (2008) 1919–1926.

[51] Y. Dong, C. Feng, P. Jiang, G. Wang, K. Li, H. Miao, Simple one-pot synthesis of ZnO/Ag heterostructures and the application in visible-light-responsive photocatalysis, RSC Adv., 4 (2014) 7340–7346.
[52] D.H. Zhang, Z.H. Xue, Q.P. wang, The mechanisms of blue emission from ZnO films deposited on glass substrate by r.f. magnetron sputtering, J. Phys. D: Appl. Phys., 35 (2002) 2837–2840.
[53] A.K. Zak, R. Razali, W.H. Abd Majid, M. Darroudi, Synthesis and characterization of a narrow size distribution of zinc oxide nanoparticles, Int. J. Nanomed., 6 (2011) 1399–1403.
[54] D. Segets, J. Gradl, R.K. Taylor, V. Vassilev, W. Peukert, Analysis of optical absorbance spectra for the determination of ZnO nanoparticle size distribution, solubility, and surface energy, ACS Nano, 3 (2009) 1703–1710.
[55] K.F. Lin, H.M. Cheng, H.C. Hsu, L.J. Lin, W.F. Hsieh, Band gap variation of size-controlled ZnO quantum dots synthesized by sol–gel method, Chem. Phys. Lett., 208 (2005) 409–413.
[56] N. Bala, S. Saha, M. Chakraborty, M. Maiti, S. Das, R. Basu, P. Nandy, Green synthesis of zinc oxide nanoparticles using *Hibiscus subdariffa* leaf extract: effect of temperature on synthesis, anti-bacterial activity and anti-diabetic activity, RSC Adv., 5 (2015) 4993–5003.
[57] P. Zhang, F. Xu, A. Navrotsky, J.S. Lee, S. Kim, J. Liu, Surface enthalpies of nanophase ZnO with different morphologies, Chem. Mater., 19 (2007) 5687–5693.
[58] M. McDonald, I. Mila, A. Scalbert, Precipitation of metal ions by plant polyphenols: optimal conditions and origin of precipitation, J. Agric. Food Chem., 44 (1996) 599–606.
[59] Q. Liu, M. Zhang, Z.X. Fang, X.H. Rong, Effects of ZnO nanoparticles and microwave heating on the sterilization and product quality of vacuum-packaged Caixin, J. Sci. Food Agric., 94 (2014) 2547–2554.
[60] WHO, Guidelines for Drinking-Water Quality, 4th ed., World Health Organization, Geneva, 2011.
[61] N.R. Jana, H. Yu, E.M. Ali, Y. Zheng, J.Y. Ying, Controlled photostability of luminescent nanocrystalline ZnO solution for selective detection of aldehydes, Chem. Commun., 14 (2007) 1406–1408.
[62] T. Yoshida, Leaching of zinc oxide in acidic solution, Mater. Trans., 4 (2003) 2489–2493.
[63] Y. Han, D. Kim, G. Hwang, B. Lee, I. Eom, P.J. Kim, M. Tong, H. Kim, Aggregation and dissolution of ZnO nanoparticles synthesized by different methods: influence of ionic strength and humic acid, Colloids Surf., A, 451 (2014) 7–15.
[64] A. Sedlak, W. Janusz, Specific adsorption of carbonate ions at the zinc oxide/electrolyte solution interface, Physicochem. Probl. Miner. Proc., 42 (2008) 57–66.
[65] T. Joseph, B. Dubey, E.A. McBean, A critical review of arsenic exposures for Bangladeshi adults, Sci. Total Environ., 528 (2015) 540–551.
[66] S. Lagergren, Zur theorie der sogenannten adsorption gelˆster stoffe, Kungliga Svenska Vetenskapsakademiens, Handlingar, 24 (1898) 1–39.
[67] Y.S. Ho, G. McKay, Pseudo-second order model for sorption processes, Process Biochem., 34 (1999) 451–465.
[68] Y.S. Ho, Review of second-order models for adsorption systems, J. Hazard. Mater., 136 (2006) 681–689.
[69] Y. Liu, New insights into pseudo-second-order kinetic equation for adsorption, Colloids Surf., A, 320 (2008) 275–278.
[70] I. Langmuir, The adsorption of gases on plane surfaces of glass, mica and platinum, J. Am. Chem. Soc., 40 (1918) 1361–1403.
[71] K.R. Hall, L.C. Eagleton, A. Acrivos, T. Vermeulen, Pore- and solid-diffusion kinetics in fixed-bed adsorption under constant-pattern conditions, Ind. Eng. Chem. Fundam., 5 (1966) 212–223.
[72] H. Freundlich, Uber die Adsorption in Losungen, Z. Phys. Chem., 57 (1907) 385–470.